Geochemical study of air quality in areas affected by the addition of anthropogenic and natural contaminants

Rebecca Biagi
Department of Earth Sciences, University of Firenze, Via G. La Pira 4 , 50121, Firenze
DOI: 10.19276/plinius.2025.01.002

INTRODUCTION

Air pollution can be defined as the alteration of the atmosphere's natural balance by introducing chemical, physical, or biological agents, in gaseous, liquid, or solid forms, resulting in health risks and environmental damage. The World Health Organization (WHO) reports that 99% of the global population breathes polluted air, contributing to millions of deaths annually and harming ecosystems (Grantz et al., 2003), crops (Vlachokostas et al., 2010), and biodiversity (Finizio et al., 1998). Air pollution also contributes to climate change through emissions of greenhouse gases (GHGs) and short-lived pollutants (IPCC, 2021).

Monitoring air pollution is complex due to *i)* the variety of sources, both natural (*e.g.*, volcanoes, wildfires, sea spray, wetlands) and anthropogenic activities (mainly in urban and industrial settings), with the latter causing rapid and severe changes, and *ii)* atmospheric processes that affect pollutant dispersion and transformation.

Traditional monitoring methods are accurate but expensive and limited in coverage. Recently, mobile and low-cost air quality stations have emerged as promising alternatives. Mobile stations provide high-resolution spatial data (*e.g.*, Apte et al., 2017; deSouza et al., 2020), while low-cost fixed sensors offer broader deployment (Clements et al., 2017; Spinelle et al., 2017; Sun et al., 2017), though they require careful calibration to ensure data quality (Heimann et al., 2015; Spinelle et al., 2017; Biagi et al., 2024).

This study proposes a combined monitoring strategy using high-tech mobile units and low-cost fixed stations to measure key pollutants (CO_2, CH_4, PM, H_2S, SO_2) and isotopic ratios ($\delta^{13}C$ of CO_2 and CH_4) in areas with overlapping natural and human sources. The method was tested in volcanic, wetland, and urban-industrial environments, demonstrating its potential for improving air quality assessments and supporting climate-related research.

CASE STUDIES: FROM NATURAL TO ANTHROPOGENIC SOURCES

Volcanic-hydrothermal areas

Vulcano Island (hereafter VU) stands as the southernmost subaerial active volcano in the Aeolian Archipelago (Southern Italy). Following the last eruption in 1888–1890 (De Astis et al., 1997) VU has been marked by intense degassing activity with *i)* high-temperature fumaroles (< 400°C after 2016) in the northern part of the La Fossa crater, with the typical composition from active volcanic systems (Nuccio et al., 1999), and *ii)* low-temperature fumaroles (< 100°C) and boiling and bubbling pools in the Baia di Levante area, reflecting the typical compositions of hydrothermal systems (Chiodini et al., 1995; Randazzo et al., 2024).

In September 2021, a new episode of volcanic unrest occurred, peaking at the end of October-early November 2021. The volcanic gas hazard on the island caused some health concerns and led to the interdiction of the crater, as well as that of the Baia di Levante beach (Mayor's ordinance n. 46/2022).

Pozzuoli (Southern Italy; hereafter PZ), located within the Campi Flegrei caldera, is a notable example of dense human settlements coexisting with an active volcanic system. The most recent eruptive activity occurred in 1538 A.D. (Monte Nuovo eruption; Orsi et al., 1996), while bradyseismic crises occurred in 1970–72 and 1982–84, when PZ was affected by a rapid ground inflation, causing uplifts up to 3.5 m (De Vivo et al., 2001). A new phase of unrest and inflation started in 2005 and is still ongoing.

The Campi Flegrei caldera is currently showing intense hydrothermal activity (Caliro et al., 2007), mostly affecting two sites: *i)* the Solfatara Crater, a 1.4 km^2-wide tuff cone produced about 4 ka from a low-magnitude eruption (Isaia et al., 2009), that hosts prominent hydrothermal discharges; *ii)* Pisciarelli, a 0.03 km^2 fault-related hydrothermal area located at the base of the Solfatara cone (approximately 400 m eastward), characterized by

high-flow fumaroles and boiling pools. Weak fumaroles and hydrothermal diffuse emissions also occur along Antiniana Street, a densely urbanized sector of the Campi Flegrei caldera located 1 km south of Pisciarelli, in the Agnano crater, where two wells were drilled for geothermal prospection.

Wetland: Padule di Fucecchio

The Padule di Fucecchio (Central Italy; hereafter FU) is the largest inner wetland (1,800 hectares) in Italy and is included in the list of wetlands of international importance under the Ramsar Convention (Ministerial Decree 303/2013). During the last centuries, the area has undergone significant hydrological changes, mainly due to anthropogenic activities, which modified the natural outflow of water for reclamation purposes (De Martin Mazzalon, 2017) and degraded the quality of the water bodies (ARPAT, 2014).

A ring of small nuclei and rural villages surrounds the FU shores, which are dominated by agricultural practices. Moving northward, the plain exhibits dense urbanization and industrialization characteristics. FU bears the impact of this anthropogenic pressure: among the critical issues are the scarce quantity and quality of water resources in spring and summer seasons, and the hunting management of marsh vegetation, which lead to a frequent manifestation of eutrophication phenomena that negatively influence the maintenance of the wetland (*e.g.*, ARPAT, 2014).

Anthropogenic sources in urban and industrial areas: a CO_2 production plant

A CO_2 production plant was selected near Sant'Albino village (hereafter SA), a residential area of approximately 2,000 inhabitants in southern Tuscany (Central Italy). The area is characterized by the emergence of bubbling pools rich in CO_2, which are fed by the deepest carbonate units hosting water and CO_2 reservoirs (Hernández-Rodríguez et al., 2017). The CO_2 discharges from these bubbling pools have been estimated at up to 100 tons day^{-1} of CO_2, while the rate of CO_2 extracted by the facility is 96 tons day^{-1} (Frondini et al., 2008; Hernández-Rodríguez et al., 2017).

From February 21 to March 12, 2023, an extraordinarily high-flux discharge activity of unfiltered CO_2 and H_2S-dominated gas was released from two chimneys of the plant, during exceptional maintenance of the waste gas cleaning apparatus, to assess the potential impact of unusual emissions on the local inhabitants.

MATERIALS AND METHODS

Mobile monitoring

CO_2, CH_4, H_2S, and SO_2 concentrations, and $\delta^{13}C_{CO_2}$ and $\delta^{13}C_{CH_4}$ values, were measured along transects within the study areas using a mobile station hosting high-tech instruments (S-volatile species were not measured at FU), following a well-established strategy to evaluate the spatial distribution of air contaminants in areas with natural (Cabassi et al., 2017) and/or anthropogenic (Vaselli et al., 2013) emissions.

The CO_2 and CH_4 concentrations, and the $\delta^{13}C_{CO_2}$ and $\delta^{13}C_{CH_4}$ values, were measured by Wavelength-Scanned Cavity Ring-Down Spectroscopy using a Picarro G2201-i analyzer. The operating interval ranged from 380 to 2,000 ppm for CO_2, and from 1.80 to 15.0 ppm for CH_4. Calibration was performed at the beginning of each measuring period. The precision was within 0.2 ppm (CO_2), 0.05 ppm (CH_4), 0.16‰ vs. V-PDB ($\delta^{13}C_{CO_2}$), and 1.15‰ vs. V-PDB ($\delta^{13}C_{CH_4}$). A copper-shavings trap was installed at the analyzer inlet port when H_2S concentrations above background values were expected (*i.e.*, VU, PZ, and SA) to minimize spectral interferences, which may result in significant depletion in ^{13}C (Malowany et al., 2015).

The H_2S and SO_2 concentrations were measured by Pulsed Fluorescence using a Thermo 450i analyzer. The instrument, which operates in the range 1-15,000 ppb, was calibrated at the beginning of the measuring periods. The precision was within ±1%.

Both instruments were housed in the back of a car moving at an average speed of ~30 km h^{-1}. Air was drawn through vacuum pumps with sampling rates of 25 mL min^{-1} and 70 mL min^{-1} for the Picarro and the Thermo devices, respectively, through 1.5 m long silicon tubes (3 mm diameters) installed on the top of the vehicle (ca. 1.80 m from the ground) to avoid the interference of exhausting gases. The Geo Tracker application, available for Android devices, was used to relate the measured parameters to the location.

The transects were selected by considering the nature and location of potential contaminant sources.

Fixed monitoring

Monitoring surveys at fixed sites were performed using low-cost multiparametric stations developed by the Department of Earth Sciences of the University of Florence (Biagi et al., 2024).

At VU, PZ, and SA, they were equipped with: *i)* a non-dispersive infrared CO_2 sensor (Sensirion SCD30); *ii)* an optical laser counting sensor for $PM_{2.5}$ and PM_{10} (Nova Fitness SDS011); and *iii)* a thermistor and a capacitive humidity sensor for T and RH, respectively (Adafruit DHT22). At FU, metal oxide semiconductor sensors for CH_4 (Figaro NGM2611-E13) were integrated, as CH_4 is one of the primary GHGs emitted by wetlands.

The CO_2 and CH_4 sensors were calibrated with a machine-learning algorithm, according to the procedure

described by Biagi et al. (2024), providing measurements with mean absolute errors < 4 ppm and < 0.03 ppm for CO_2 and CH_4, respectively. Regarding PM concentrations, several studies demonstrated generally reliable performances of this sensor compared to reference instruments (*e.g.*, Božilov et al., 2022), with very low inter-unit variability (Brugnone et al., 2024; Tagle et al., 2020). To assess the repeatability of the $PM_{2.5}$ and PM_{10} measurements across sensors, an Intraclass Correlation Coefficient (ICC) analysis was performed, obtaining excellent sensor concordance with values of 0.983 for $PM_{2.5}$ and 0.966 for PM_{10}.

The low-cost multiparametric stations were fixed at 1.5 m height, corresponding to the average breathing height of standing humans. The number of monitoring sites and their location were commensurate with the extension of the study areas and the presence of potential sources.

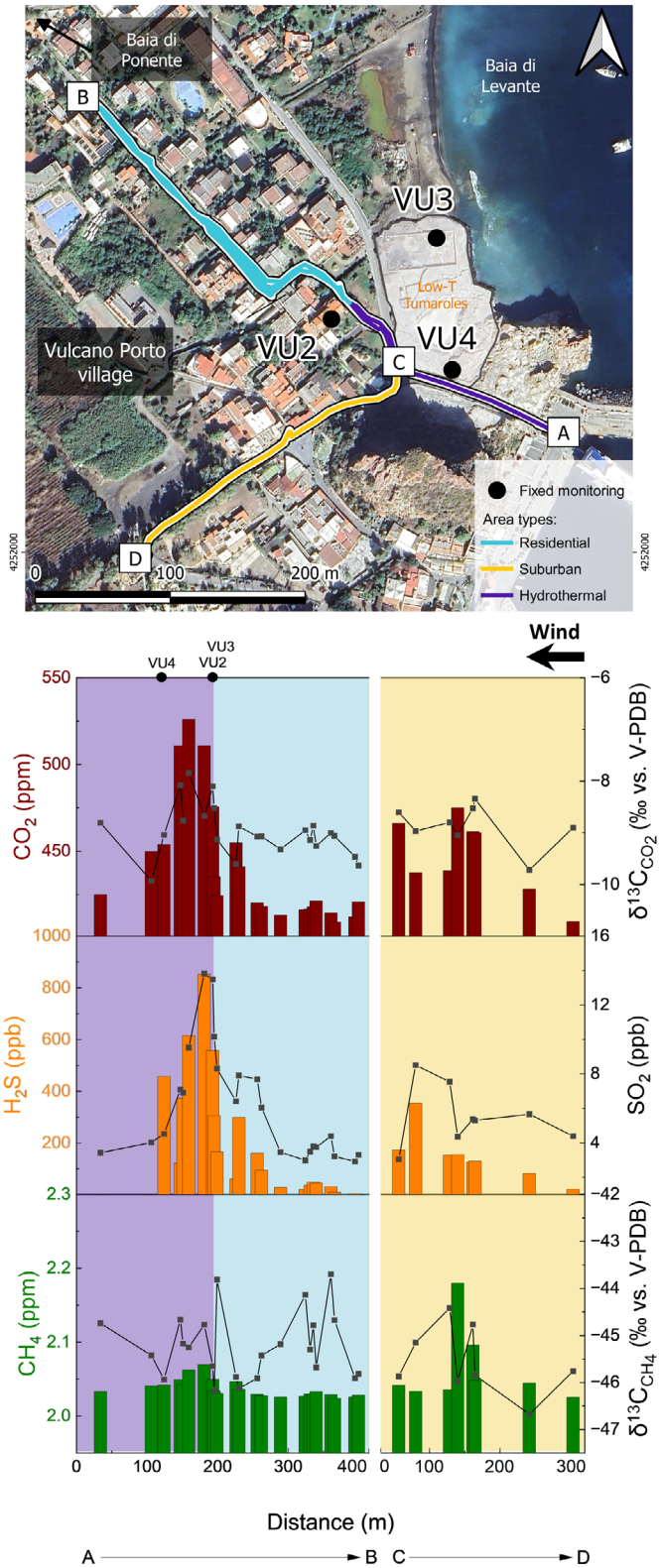

*Figure 1 Spatial distribution of CO_2, H_2S, and CH_4 concentrations (bars) and $\delta^{13}C_{CO_2}$, SO_2, and $\delta^{13}C_{CH_4}$ values (line + scatter) along the VU study area (**a,b** and **c,d**), plotted against the distance from the starting point (x-axis). Colored sections on the map and plot represent different area types (i.e., residential, suburban, and hydrothermal). Fixed monitoring sites (VU2-4), wind direction, and low-T fumaroles are also shown.*

RESULTS AND DISCUSSION

The proposed monitoring strategy yielded a high-resolution dataset (1 data point per minute), comprising approximately 1,150,000 data points from fixed monitoring and 1,100 data points from mobile monitoring.

Vulcano Island (VU)

At VU, mobile monitoring revealed significant short-distance variations in atmospheric CO_2 concentrations, reaching up to 536 ppm near the hydrothermal emissions in the Baia di Levante (Fig. 1). None of the measured CO_2 levels posed health risks based on short-term (NIOSH, 2014), occupational (OSHA, 2024), or chronic exposure standards (Martrette et al., 2017).

H_2S levels peaked at 882 ppb along the same transect, following a similar trend as CO_2 (Fig. 1). Though H_2S concentrations decreased away from the source, they remained above the 10-ppb odor threshold (WHO, 2003). However, they were well below levels associated with health impacts (≥ 90 ppb) (Batterman et al., 2023).

Isotopic analysis and theoretical mixing models (Keeling plot; Keeling, 1961) confirmed that the primary source of CO_2 and H_2S was related to the hydrothermal emissions of the Baia di Levante, although some CO_2 enrichment suggested minor anthropogenic contributions, likely from fossil fuel combustion (Fig. 2a, b). A strong correlation between H_2S and SO_2 supported oxidation-driven transformations in the air (Pearson's r: 0.84).

CH_4 concentrations (2.02–2.18 ppm) mirrored the spatial patterns of CO_2 and H_2S, likely indicating their common hydrothermal origin (Fig. 1). However, isotopic data did not clearly identify the signature of the CH_4 source (Fig. 2c), and a few CH_4 anomalies indicated possible unidentified anthropogenic contributions (Fig. 2d).

Fixed-site monitoring, combined with wind direction data, further helped in identifying the main sources of CO_2 and PM in the monitored sites. At Baia di Levante (VU2, VU3, VU4; Fig. 1), CO_2 concentrations (up to 835 ppm) were linked to specific wind patterns from the hydrothermal emissions. $PM_{2.5}$ and PM_{10} data exhibited complex behaviors, indicating both hydrothermal and

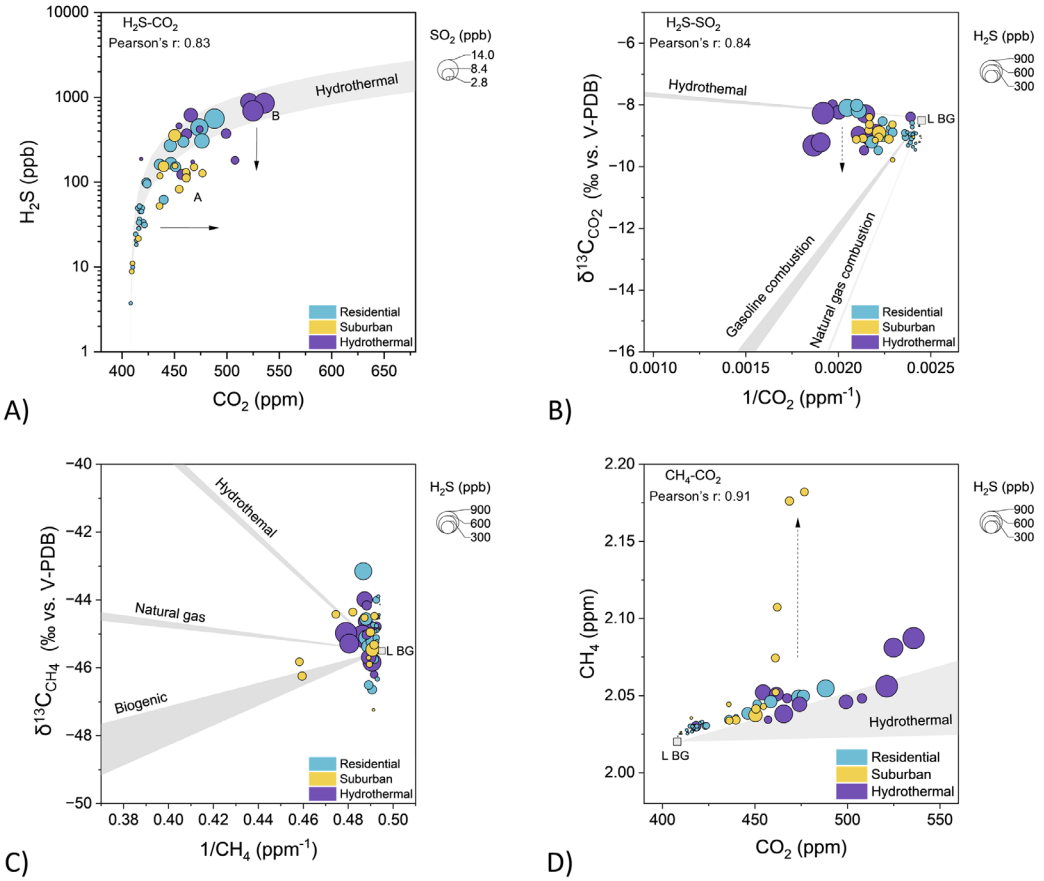

Figure 2 ***a)*** *H_2S vs. CO_2 diagram.* ***b)*** *CO_2 and* ***c)*** *CH_4 Keeling plots.* ***d)*** *CH_4 vs. CO_2 diagram. Symbol size is proportional to* ***(a)*** *SO_2 concentration and* ***(b-d)*** *H_2S concentration. Symbol colors represent the area types (i.e., residential, suburban, and hydrothermal). Gray fields represent mixing trends with theoretical sources. L BG is the chemical and isotopic composition of the local background.*

anthropogenic origins. Particularly, $PM_{2.5}$ was more often associated with hydrothermal sources, while PM_{10} appeared to be influenced by local human activities in Vulcano Porto.

Pozzuoli (PZ)

Mobile monitoring in the PZ study area revealed higher CO_2 concentrations in hydrothermal (up to 798 ppm) and urban/industrial sectors (up to 546 ppm), while values in suburban and residential zones remained closer to the 2022 global background average (~418 ppm).

H_2S concentrations were higher in hydrothermal areas (up to 364 ppb), but NE winds occasionally transported it into suburban (up to 29 ppb) and residential (up to 82 ppb) sectors. These findings indicate that hydrothermal gases can affect air quality over distances greater than 2 km from the major emission sites of La Solfatara, Pisciarelli, and Antiniana Street.

A common hydrothermal origin for CO_2 and H_2S was confirmed by mixing trends consistent with emissions from La Solfatara and Pisciarelli. However, observed CO_2 enrichments resulted from *i)* anthropogenic input (which led to lighter $\delta^{13}C_{CO_2}$ without a corresponding increase in H_2S concentrations), and/or *ii)* depletion of H_2S due to oxidation to SO_2, supported by a strong correlation between the two S-species (Pearson's r = 0.85).

CH_4 showed modest spatial variability with peaks up to 2.25 ppm, particularly in suburban areas, but lacked a clear spatial pattern. Isotopic signatures ($\delta^{13}C_{CH_4}$) and bivariate analyses suggest multiple sources (including hydrothermal, natural gas, and biogenic inputs), as well as the influence of atmospheric oxidation.

At fixed monitoring sites, CO_2 accumulation occurred primarily under low wind conditions, with directional wind analyses indicating both hydrothermal and anthropogenic influences depending on location. Particulate matter (PM) levels varied across sites, with $PM_{2.5}$ occasionally exceeding long-term WHO exposure limits (5 $\mu g\ m^{-3}$), particularly under stable atmospheric conditions and traffic influence.

While CO_2 and PM levels did not indicate immediate health risks, H_2S concentrations in a car dealership and a nursing home warrant concern due to chronic exposure risks. Estimated H_2S levels, based on H_2S/CO_2 ratios measured during the mobile monitoring, reached 49 ppb and 292 ppb, respectively, the latter representing a potential health risk for vulnerable populations.

Padule di Fucecchio (FU)

Mobile monitoring in FU showed nearly constant CO_2 concentrations (~420 ppm), while CH_4 levels decreased along the transect. The $\delta^{13}C_{CO_2}$ and $\delta^{13}C_{CH_4}$ values of a potential end-member computed using the Keeling plots analysis indicated a common biogenic source for both CO_2 (-25.5‰ vs. V-PDB) and CH_4 (-67.7‰ vs. V-PDB), consistent with microbial activity in anaerobic soil and wetland environments.

At nine fixed monitoring sites, clear diurnal cycles related to the Planetary Boundary Layer dynamics were observed: higher concentrations at night/morning un-

der stable conditions and lower values in the afternoon. Wetland sites showed greater CO_2 and CH_4 due to biogenic emissions, while upstream rural sites had lower and more stable levels. Notably, constantly higher CH_4 concentrations (2.60 ppm on average) were observed at one site inside the wetland across nearly all wind directions, likely due to the presence of several canals where eutrophic conditions may have enhanced CH_4 production.

Particulate matter showed a different distribution: $PM_{2.5}$ was higher in urban zones and transported upstream by wind, while PM_{10} was higher in the downstream wetland sites. Notably, long-term exposure thresholds for $PM_{2.5}$ were consistently exceeded at two sites, indicating a need for continued monitoring in these areas.

The CO_2 production plant (SA)

At SA, three monitoring campaigns evaluated air quality impacts from the CO_2 production plant under different operational conditions: FLD (filtered low-discharge) and UHD (unfiltered high-discharge).

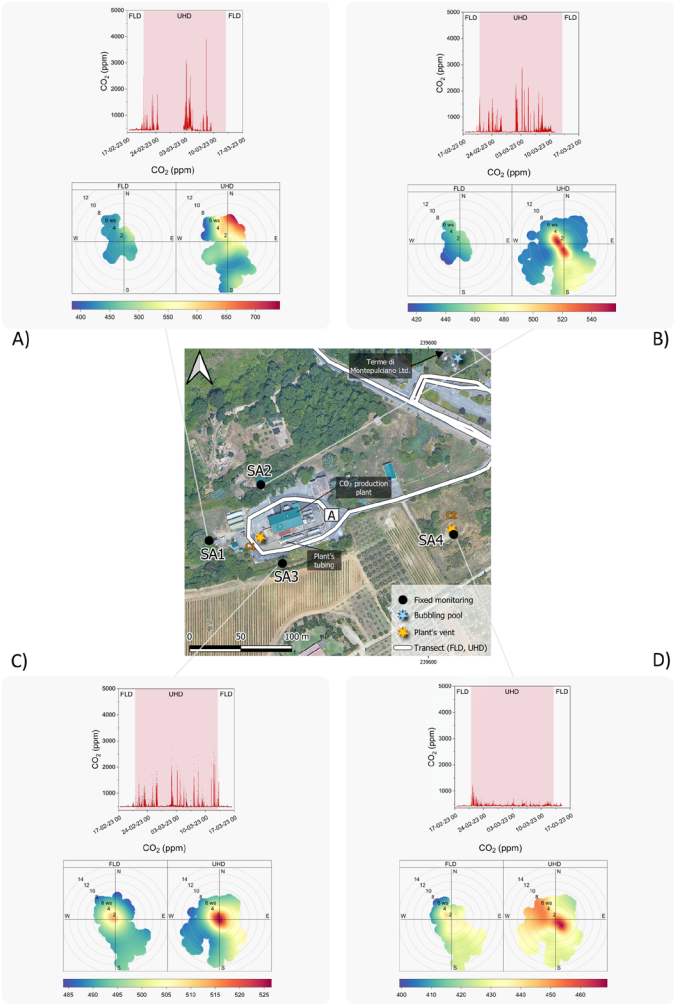

*Figure 3 Time series of CO_2 concentrations (1-minute average black point; 5-minute rolling mean red line), along with polar plots of CO_2 10-minute averaged concentrations (represented by different colors) at SA1 **(a)**, SA2 **(b)**, SA3 **(c)**, and SA4 **(d)**, divided into FLD and UHD conditions. The pink areas in the time series are the periods under UHD conditions. Fixed monitoring sites, bubbling pools, and the main plant's emitting vents (C1 and C2) are also shown.*

Under FLD conditions, CO_2 and CH_4 concentrations were generally higher in suburban and residential areas of SA, rather than near the plant, with peaks up to 495 ppm (CO_2) and 2.33 ppm (CH_4). Near the plant, levels were close to background (404 ppm CO_2, 2.02 ppm CH_4), suggesting minimal plant influence under standard operations. Instead, vehicular traffic and domestic heating in the village were likely the main contributors of CO_2 and CH_4 based on their $\delta^{13}C$ values, with a minor geogenic signal near a local bubbling pool. H_2S levels were negligible, indicating no detectable emissions from the plant under normal operation.

Under UHD conditions, a strong, localized gas anomaly was detected near the plant, with concentrations of CO_2 up to 2,000 ppm, CH_4 up to 10.5 ppm, H_2S up to 95.3 ppb, and SO_2 up to 3.44 ppb, with $\delta^{13}C$ values indicating a geogenic gas source. However, these values rapidly decreased with distance due to dilution and H_2S oxidation. Outside the immediate area, gas levels remained low with $\delta^{13}C$ values compatible with anthropogenic emissions.

At fixed sites, the three closest to the plant (SA1–SA3; Fig. 3a-c) showed CO_2 peaks under UHD conditions, especially in the early morning, matching reported gas discharge times. Site SA3 (Fig. 3c) showed elevated CO_2 even under FLD, possibly due to a local leak from plant tubing. Conversely, more distant sites (SA4 and SA5; Figs. 3d and 4, respectively) had stable CO_2 levels (~440 ppm).

$PM_{2.5}$ and PM_{10} concentrations were higher under UHD, especially near the plant, likely due to secondary particle formation from geogenic emissions. However, PM was often higher in the village (SA5) than near the plant, suggesting a stronger influence from domestic and traffic-related sources. WHO thresholds for $PM_{2.5}$ and PM_{10} were exceeded in both periods at certain sites, especially SA5.

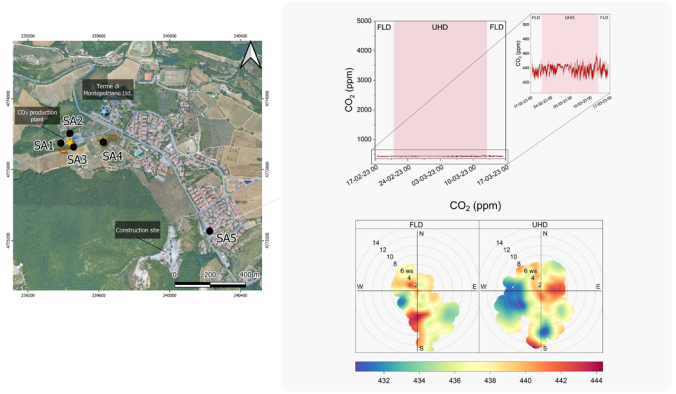

Figure 4 Time series of CO_2 concentrations (1-minute average black point; 5-minute rolling mean red line), along with polar plots of CO_2 10-minute averaged concentrations (represented by different colors) at SA5 divided into FLD and UHD conditions. The pink areas in the time series are the periods under UHD conditions. Fixed monitoring sites, bubbling pools, and the main plant's emitting vents (C1 and C2) are also shown.

Wind analysis showed that high CO_2 and PM concentrations at SA1–SA4 under UHD were associated with low wind speeds and downwind conditions from the plant, confirming plant emissions. However, at SA5, CO_2 and PM patterns did not differ between UHD and FLD, confirming local non-plant sources (*e.g.*, traffic, domestic heating, and a nearby construction site).

CONCLUSIONS

This study demonstrates that combining low-cost fixed stations with high-tech mobile systems offers an effective, adaptable, and affordable approach to air quality monitoring across diverse environments, including volcanic, wetland, urban, and industrial areas.

Fixed stations enabled continuous tracking of pollutants like CO_2, CH_4, $PM_{2.5}$, and PM_{10}, capturing variability due to weather and emission sources. Their affordability and improved calibration allowed for denser networks and better spatial resolution, especially in underserved regions. Mobile systems complemented this with broader spatial coverage and detailed source identification using isotopic analysis.

While challenges remain, such as limited long-term sensor calibration and the labor-intensive nature of mobile surveys, the integrated approach enhances monitoring capabilities, supports research and policy, and is suitable for citizen science. Its scalability makes it ideal for at-risk areas, with future potential for drone integration to access hazardous or hard-to-reach sites.

REFERENCES

Apte, J.S., Messier, K.P., Gani, S., Brauer, M., Kirchstetter, T.W., Lunden, M.M., Marshall, J.D., Portier, C.J., Vermeulen, R.C.H., Hamburg, S.P. (2017) - High-Resolution Air Pollution Mapping with Google Street View Cars: Exploiting Big Data. Environ. Sci. Technol., 51, 6999–7008.

ARPAT (2014) - Valutazione della qualità ambientale del Padule di Fucecchio Aggiornamento 2013 Report ARPAT Dipartimento provinciale ARPAT di Pistoia.

Avnery, S., Mauzerall, D.L., Liu, J., Horowitz, L.W. (2011) - Global crop yield reductions due to surface ozone exposure: 1. Year 2000 crop production losses and economic damage. Atmos. Environ., 45, 2284–2296.

Batterman, S., Grant-Alfieri, A., Seo, S.-H. (2023) - Low level exposure to hydrogen sulfide: a review of emissions, community exposure, health effects, and exposure guidelines. Crit. Rev. Toxicol., 53, 244–295.

Biagi, R., Ferrari, M., Venturi, S., Sacco, M., Montegrossi, G., Tassi, F. (2024) - Development and machine learning-based calibration of low-cost multiparametric stations for the measurement of CO_2 and CH_4 in air. Heliyon, 10.

Božilov, A., Tasić, V., Živković, N., Lazović, I., Blagojević, M., Mišić, N., Topalović, D. (2022) - Performance assessment of NOVA SDS011 low-cost PM sensor in various microenvironments. Environ. Monit. Assess., 194, 595.

Brugnone, F., Randazzo, L., Calabrese, S. (2024) - Use of Low-Cost Sensors to Study Atmospheric Particulate Matter Concentrations: Limitations and Benefits Discussed through the Analysis of Three Case Studies in Palermo, Sicily. Sensors, 24, 6621.

Cabassi, J., Tassi, F., Venturi, S., Calabrese, S., Capecchiacci, F., D'Alessandro, W., Vaselli, O. (2017) - A new approach for the measurement of gaseous elemental mercury (GEM) and H_2S in air from anthropogenic and natural sources: Examples from Mt. Amiata (Siena, Central Italy) and Solfatara Crater (Campi Flegrei, Southern Italy). J. Geochem. Explor., 175, 48–58.

Caliro, S., Chiodini, G., Moretti, R., Avino, R., Granieri, D., Russo, M., Fiebig, J. (2007) - The origin of the fumaroles of La Solfatara (Campi Flegrei, South Italy). Geochim. Cosmochim. Acta, 71, 3040–3055.

Chiodini, G., Cioni, R., Marini, L., Panichi, C. (1995) - Origin of the fumarolic fluids of Vulcano Island, Italy and implications for volcanic surveillance. Bull. Volcanol., 57, 99–110.

Clements, A.L., Griswold, W.G., Abhijit, R.S., Johnston, J.E., Herting, M.M., Thorson, J., Collier-Oxandale, A., Hannigan, M. (2017) - Low-cost air quality monitoring tools: From research to practice (A workshop summary). Sensors (Switzerland).

De Astis, G., La Volpe, L., Peccerillo, A., Civetta, L. (1997) - Volcanological and petrological evolution of Vulcano island (Aeolian Arc, southern Tyrrhenian Sea). J. Geophys. Res. Solid Earth, 102, 8021–8050.

De Martin Mazzalon, M. (2017) - Inquadramento idrogeologico del Padule di Fucecchio. In: "Guida del Padule di Fucecchio. Natura, storia, tradizioni, itinerari. Quaderni del Padule di Fucecchio N.8.", A. Bartolini, G. Calvetti, L. Candiani, M. De Martin Mazzalon, A. Lucci, A. Malvolti, E. Zarri, eds. Centro di Ricerca, Documentazione e Promozione del Padule di Fucecchio.

De Vivo, B., Rolandi, G., Gans, P.B., Calvert, A., Bohrson, W.A., Spera, F.J., Belkin, H.E. (2001) - New constraints on the pyroclastic eruptive history of the Campanian volcanic Plain (Italy). Miner. Petrol., 73, 47-65.

deSouza, P., Anjomshoaa, A., Duarte, F., Kahn, R., Kumar, P., Ratti, C. (2020) - Air quality monitoring using mobile low-cost sensors mounted on trash-trucks: Methods development and lessons learned. Sustain. Cities Soc., 60, 102239.

Finizio, A., Di Guardo, A., Cartmale, L. (1998) - Hazardous Air Pollutants (HAPs) and their Effects on Biodiversity: An Overview of the Atmospheric Pathways of Persistent Organic Pollutants (POPs) and Suggestions for Future Studies. Environ. Monit. Assess., 49, 327–336.

Frondini, F., Caliro, S., Cardellini, C., Chiodini, G., Morgantini, N., Parello, F. (2008) - Carbon dioxide degassing from Tuscany and Northern Latium (Italy). Global Planet. Change, 61, 89–102.

Grantz, D.A., Garner, J.H.B., Johnson, D.W. (2003) - Ecological effects of particulate matter. Environ. Int., 29, 213-239.

Heimann, I., Bright, V.B., McLeod, M.W., Mead, M.I., Popoola, O.A.M., Stewart, G.B., Jones, R.L. (2015) - Source attribution of air pollution by spatial scale separation using high spatial density networks of low cost air quality sensors. Atmos. Environ., 113, 10–19.

Hernández-Rodríguez, A., Montegrossi, G., Huet, B., Vaselli, O., Virgili, G. (2017) - A study of wellbore cement alteration controlled by CO_2 leakage in a natural analogue for geological CO_2 storage. Appl. Geochem., 86, 13–25.

IPCC (2021) - Climate Change 2021: The Physical Science Basis. Cambridge University Press.

Isaia, R., Marianelli, P., Sbrana, A. (2009) - Caldera unrest prior to intense volcanism in Campi Flegrei (Italy) at 4.0 ka B.P.: Implications for caldera dynamics and future eruptive scenarios. Geophys. Res. Lett., 36.

Keeling, C.D. (1961) - The concentration and isotopic abundances of carbon dioxide in rural and marine air. Geochim. Cosmochim. Acta, 24, 277–298.

Malowany, K., Stix, J., Van Pelt, A., Lucic, G. (2015) - H_2S interference on CO_2 isotopic measurements using a Picarro G1101-i cavity ring-down spectrometer. Atmos. Meas. Tech., 8, 4075–4082.

Martrette, J.M., Egloff, C., Clément, C., Yasukawa, K., Thornton, S.N., Trabalon, M. (2017) - Effects of prolonged exposure to CO_2 on behaviour, hormone secretion and respiratory muscles in young female rats. Physiol. Behav., 177, 257–262.

NIOSH (2014) - Carbon dioxide [WWW Document]. URL: https://www.cdc.gov/niosh/idlh/124389.html#print (accessed 1.8.25).

Nuccio, P.M., Paonita, A., Sortino, F. (1999) - Geochemical modeling of mixing between magmatic and hydrothermal gases: the case of Vulcano Island, Italy. Earth Planet. Sci. Lett., 167, 321–333.

Orsi, G., De Vita, S., Di Vito, M. (1996) - The restless, resurgent Campi Flegrei nested caldera (Italy): constraints on its evolution and configuration. J. Volcanol. Geoth. Res., 74, 179-214.

OSHA (2024) - CARBON DIOXIDE [WWW Document]. URL: https://www.osha.gov/chemicaldata/183 (accessed 11.15.24).

Randazzo, A., Venturi, S., Tassi, F. (2024) - Soil processes modify the composition of volatile organic compounds (VOCs) from CO_2- and CH_4-dominated geogenic and landfill gases: A comprehensive study. Sci. Total Environ., 923.

Schulze, E.-D. (1989) - Air Pollution and Forest Decline in a Spruce (Picea abies) Forest. Science, 244, 776–783.

Spinelle, L., Gerboles, M., Villani, M.G., Aleixandre, M., Bonavitacola, F. (2017) - Field calibration of a cluster of low-cost commercially available sensors for air quality monitoring. Part B: NO, CO and CO_2. Sens. Actuators B Chem., 238, 706–715.

Sun, L., Westerdahl, D., Ning, Z. (2017) - Development and evaluation of a novel and cost-effective approach for low-cost NO2 sensor drift correction. Sensors (Switzerland), 17.

Tagle, M., Rojas, F., Reyes, F., Vásquez, Y., Hallgren, F., Lindén, J., Kolev, D., Watne, Å.K., Oyola, P. (2020) - Field performance of a low-cost sensor in the monitoring of particulate matter in Santiago, Chile. Environ. Monit. Assess., 192.

Van Dingenen, R., Dentener, F.J., Raes, F., Krol, M.C., Emberson, L., Cofala, J. (2009) - The global impact of ozone on agricultural crop yields under current and future air quality legislation. Atmos. Environ., 43, 604–618.

Vaselli, O., Higueras, P., Nisi, B., María Esbrí, J., Cabassi, J., Martínez-Coronado, A., Tassi, F., Rappuoli, D. (2013) - Distribution of gaseous Hg in the Mercury mining district of Mt. Amiata (Central Italy): A geochemical survey prior the reclamation project. Environ. Res., 125, 179–187.

Vlachokostas, Ch., Nastis, S.A., Achillas, Ch., Kalogeropoulos, K., Karmiris, I., Moussiopoulos, N., Chourdakis, E., Banias, G., Limperi, N. (2010) - Economic damages of ozone air pollution to crops using combined air quality and GIS modelling. Atmos. Environ., 44, 3352–3361.

WHO (2003) - Hydrogen sulfide: human health aspects. World Health Organization, Geneva.